Electronic Supplementary Material (ESI) for New Journal of Chemistry.

Supporting information

The NiCo alloy synergistic Pt nanocatalyst for enhancing the durability of methanol oxidation reaction

Feng Luo,[1] Tingyi Wen,[1] Jiarui Wu,[1] Hao qing Qin,[1] Xiaoqiang Wu,[1,2*]

1. School of Mechanical Engineering, Chengdu University, Chengdu 610106, China
2. Material Corrosion and Protection Key Laboratory of Sichuan province, Sichuan University of Science & Engineering

Correspondence and requests for materials should be addressed to XQ.W (email: wuxiaoqiang@cdu.edu.cn).

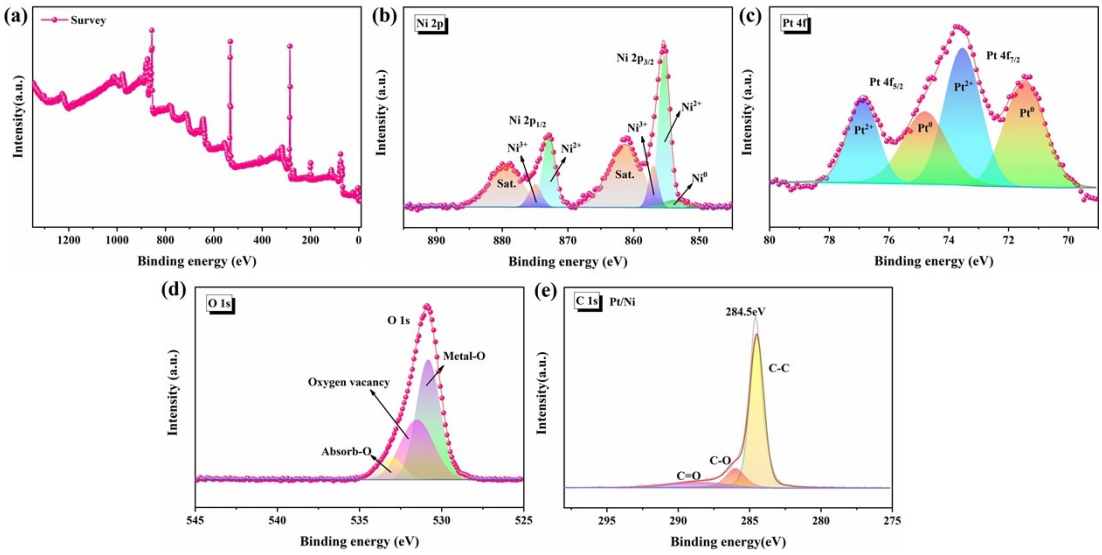

Fig.S1 XPS analysis of Pt/Ni. (a) Survey. (b) Ni 2p. (c) Pt 4f. (d) O 1s. (e) C 1s.

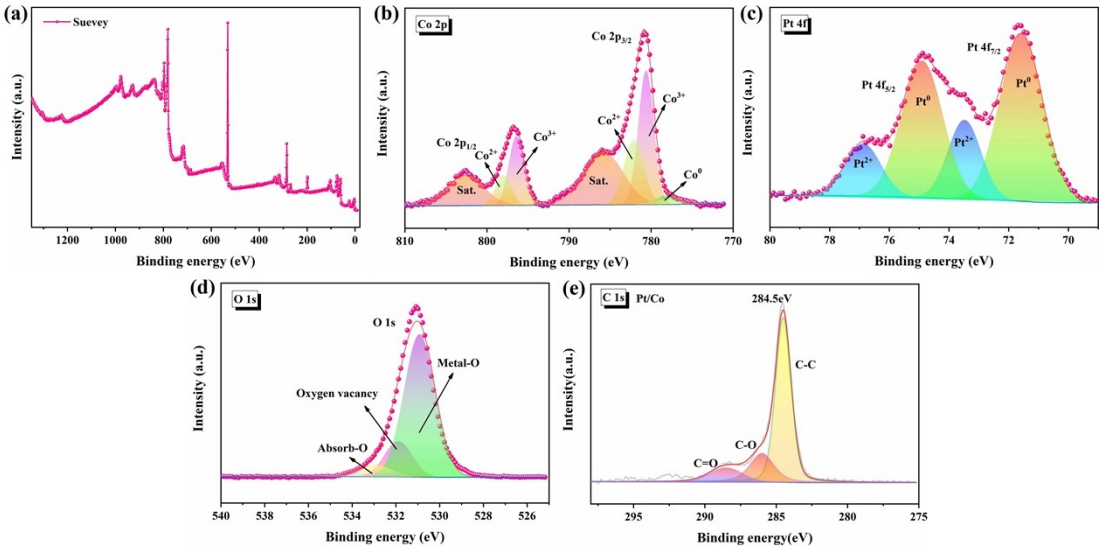

Fig.S2 XPS analysis of Pt/Co. (a) Survey. (b) Ni 2p. (c) Pt 4f. (d) O 1s. (e) C 1s.

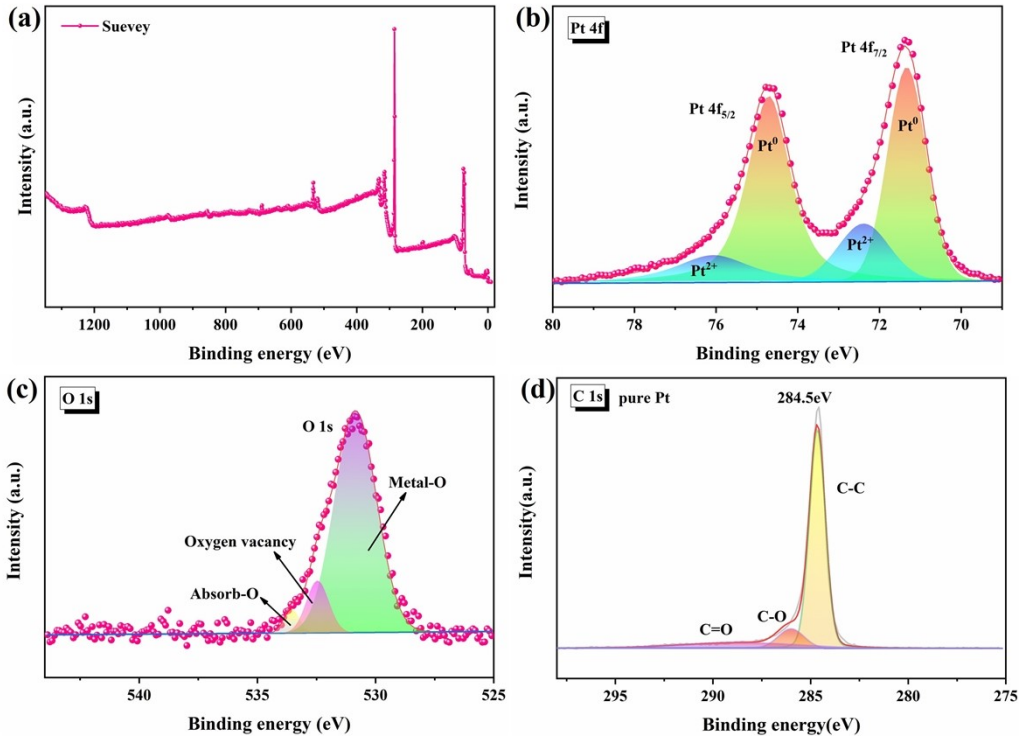

Fig.S3 XPS analysis of pure Pt. (a) Survey. (b) Pt 4f. (c) O 1s. (d) C 1s.

Fig.S1-S3 show the X-ray photoelectron spectra (XPS) of different samples Pt/Ni, Pt/Co, and pure Pt. The full spectrum of **Fig.S1a** shows clear characteristic peak signals for the Ni 2p and Pt4f orbitals, with the Ni 2p orbitals having distinct peaks at 873.2 eV (Ni $2p_{1/2}$) and 855.6 eV (Ni $2p_{3/2}$), which can be attributed to Ni^{2+}, as shown in **Fig.S1b**. The valence state of platinum can be divided into two pairs of peaks to identify it, as shown in **Fig.S1c**. The peak value is approximately 71.47 eV (Pt $4f_{7/2}$), 74.8 eV (Pt $4f_{5/2}$) belongs to Pt^0, 73.54 eV (Pt $4f_{7/2}$), and 76.88 eV (Pt $4f_{5/2}$) belongs to Pt^{2+}. Similarly, Pt/Co also exhibits the same valence states of Pt including Pt^0 (Pt $4f_{7/2}$, 71.58 eV and Pt $4f_{5/2}$, 74.9 eV) and Pt^{2+} (Pt $4f_{7/2}$, 73.48 eV and Pt $4f_{5/2}$, 76.9 eV), as shown in **Fig.S2c**. Co exists mainly in the form of Co^{2+} ($Co2p_{3/2}$, 780.1 eV and $Co2p_{1/2}$, 796.3 eV) as shown in **Fig.S2b**. In addition, the photoelectron spectra of pure Pt were also measured, as shown in **Fig.S3**. Compared with the contents of Pt^{2+} (Pt $4f_{7/2}$, 72.39 eV

and Pt $4f_{5/2}$, 76.1 eV) in pure Pt,[1, 2] as shown in **Fig.S3b**, the contents of Pt^{2+} in Pt/Ni, Pt/Co and Pt/NiCo all increased. This may be because the addition of Ni or Co changed the electronic structure of Pt. Electrons are transferred from Pt to Ni or Co, and the electron interaction simultaneously increases the binding energy of Pt. The binding energy of all samples was corrected by a C1s peak (284.5eV),[3] as shown in **Fig.S1e**, **Fig.S2e**, and **Fig.S3d**.

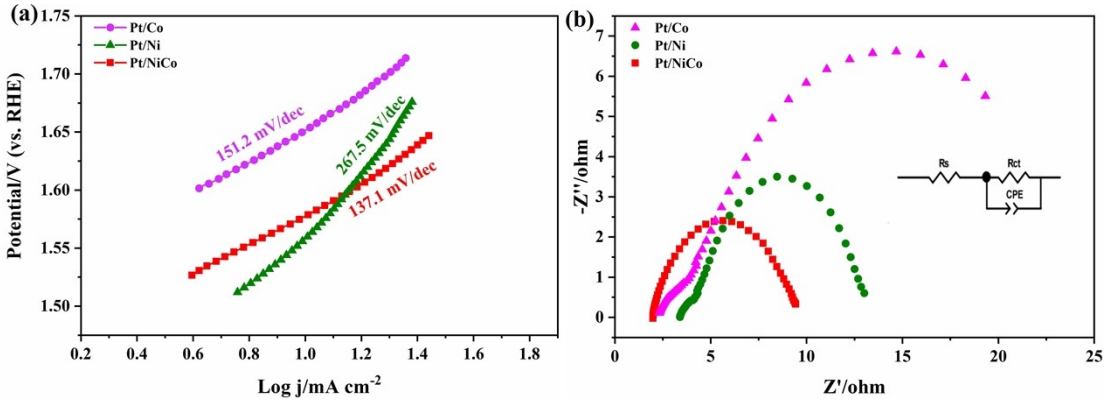

Fig.S4 (a) Tafel and (b) EIS of Pt/Ni, Pt/Co and Pt/NiCo in 1M KOH solution

Tafel slope and EIS are also used as factors to evaluate the slow OER kinetics. The Tafel slope and EIS of Pt/Ni, Pt/Co and Pt/NiCo were measured in alkaline solution, as shown in **Fig.S4**. Compared with the Tafel slope of Pt/Ni (267.5 mV /s) and Pt/Co (151.2 mV/dec), Pt/NiCo showed the lowest Tafel slope (137.1 mV /dec), as shown in **Fig.S4a**. In addition, the R_{ct} tested by EIS showed a trend of Pt/NiCo < Pt/Ni < Pt/Co, as shown in **Fig.S4b**. The above results further indicate that Pt/NiCo has better electrical conductivity and reaction rate.

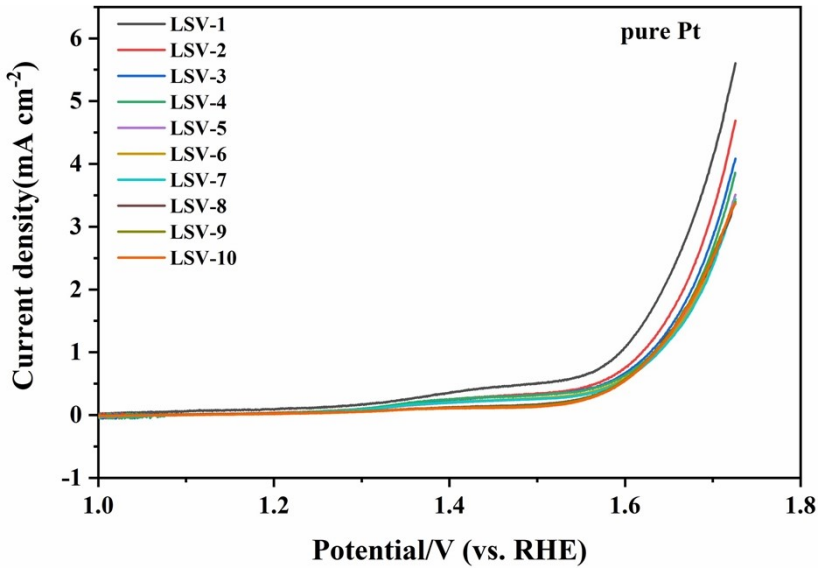

Fig.S5 The LSV curves of pure Pt in 1M KOH solution.

In order to further explore the synergistic effect of Pt and NiCo, the OER performance of pure Pt under 1M KOH alkaline solution was tested. **Fig.S5** shows the LSV curve of pure Pt with a scanning rate of 1 mV/s in 1M KOH solution. After 10 consecutive LSV measurements, the current density gradually decreased, and when the current density gradually stabilized at 2 mA cm^{-2}, the lowest overpotential could only reach 450mV, which indicates that the OER performance under the action of Pt alone is poor, and further proves the good synergistic effect of Pt and NiCo.

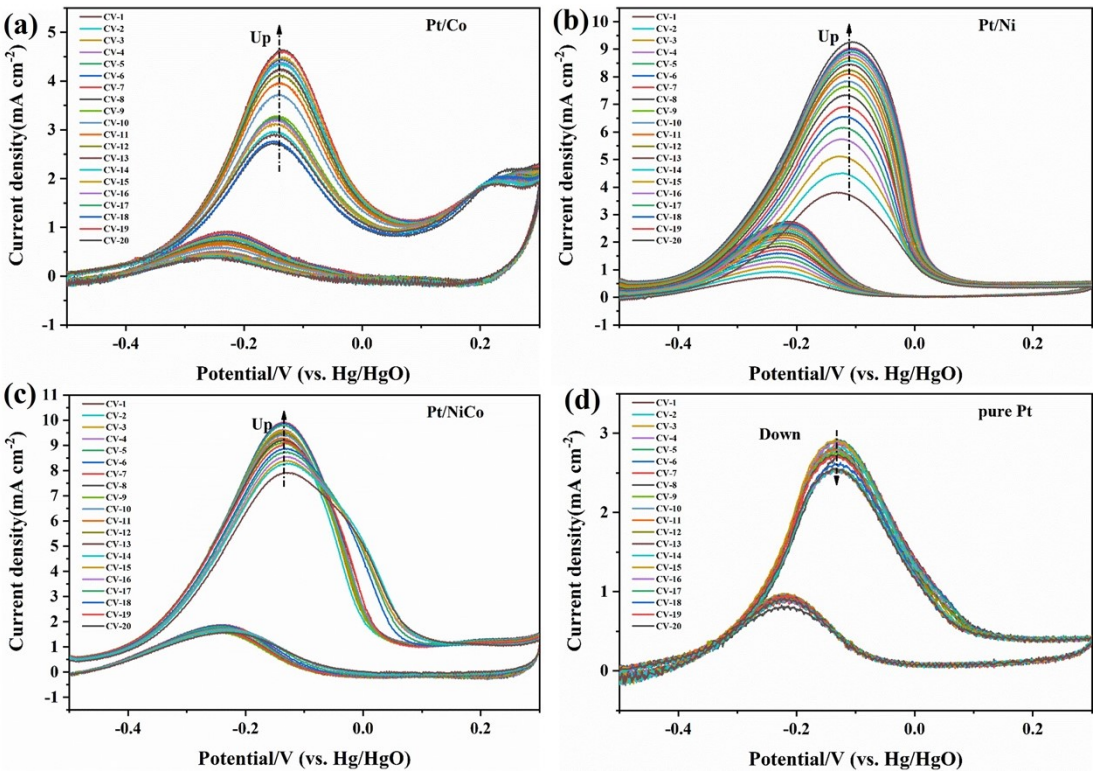

Fig.S6 Continuous CV curves of (a) Pt/Co, (b) Pt/Ni, (c) Pt/NiCo and (d) pure Pt for the first 20 times at a sweep speed of 50 mV/s in 1M KOH and 1M methanol solutions.

Fig.S6 shows the continuous CV curves of Pt/Co, Pt/Ni, Pt/NiCo and pure Pt for the first 20 times at a scanning speed of 50 mV/s in 1M KOH and 1M methanol solutions. It was found that the MOR activity of Pt/Co, Pt/Ni and Pt/NiCo catalysts gradually increased and reached a stable state during 20 scans, while that of pure Pt was in a downward trend, which was attributed to the good adaptability of Pt and other transition metals. At the same time, the MOR activity after steady state was further compared, and Pt/NiCo showed higher mass activity than other catalysts, indicating a good synergistic effect between Pt and NiCo.

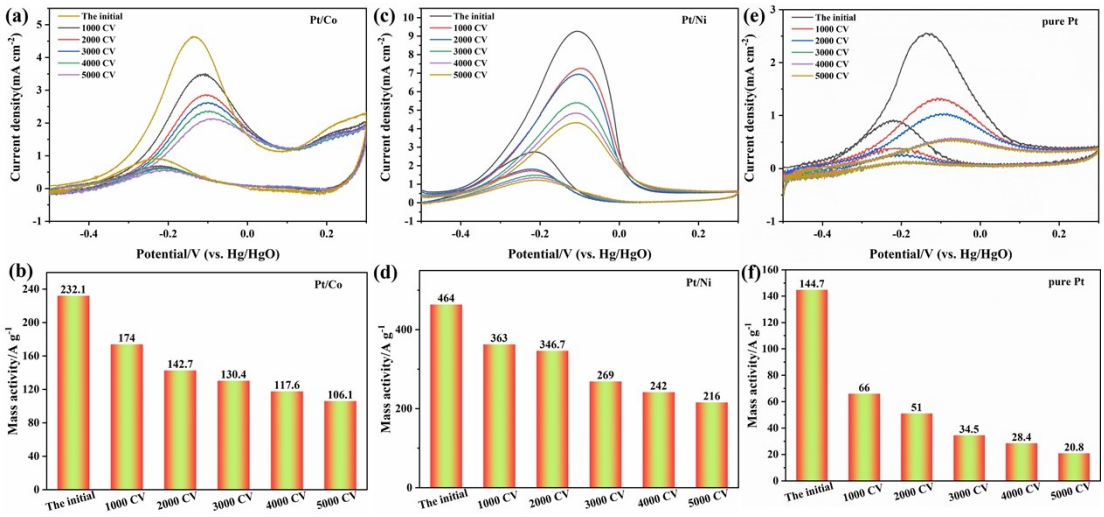

Fig.S7 CV cycle stability tests for (a-b) Pt/Co, (c-d) Pt/Ni and (e-f) pure Pt at 1000, 2000, 3000, 4000, 5000 cycles.

Stability is also an important index to evaluate the catalyst, which determines whether the catalyst can catalyze the reaction stably for a long time. **Fig.S7** shows the CV cycle stability of Pt/Co, Pt/Ni, and pure Pt. MOR mass activity was tested at 1000, 2000, 3000, 4000 and 5000 CV cycles respectively, and the results showed that the mass activity was gradually decreased. Compared with the activity after 5000 CV cycles, The trend is Pt/NiCo (315.2 A g^{-1}_{Pt}) > Pt/Ni (216 A g^{-1}_{Pt}) > Pt/Co (106.1 A g^{-1}_{Pt}) > pure Pt (20.8 A g^{-1}_{Pt}). Meanwhile, by comparing the activity decay trend of 1000 to 5000 CV cycles, it is found that pure Pt decays the fastest, while Pt/Co, Pt/Ni and Pt/NiCo decays slowly, and the final Pt/NiCo shows a low decay rate of 36.4%. The above results prove the good detoxification ability of NiCo transition metal, and also demonstrate the stronger catalytic performance of bimetal than single metal and cooperate with Pt to further improve the stability of catalyst.

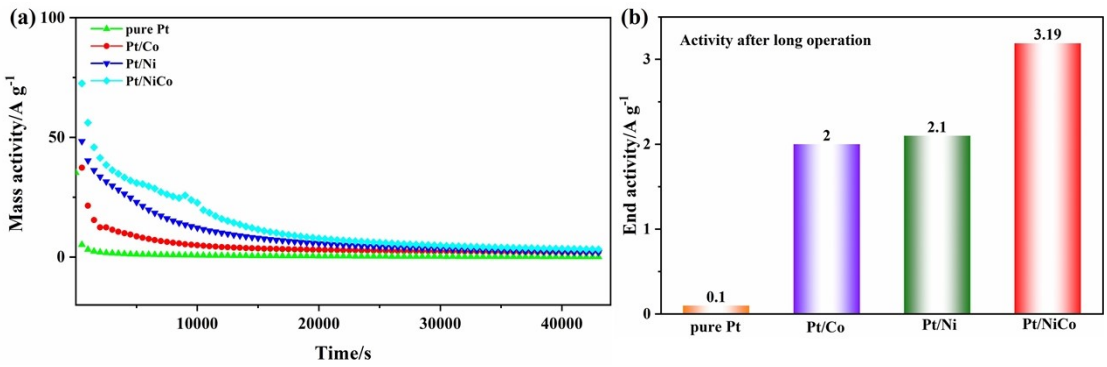

Fig.S8 Long-term operational durability testing. (a) I-t curves. (b) End activity after long operation.

Fig.S8 shows the CA curve for a longer run. The results show that after 43,200 s, Pt/NiCo showed a higher MOR termination activity (3.19 A g^{-1}_{Pt}) than Pt/Ni, Pt/Co and pure Pt. This further proves that under alkaline conditions, NiCo can further promote the dissociation of water to form *OH and improve the durability of MOR.

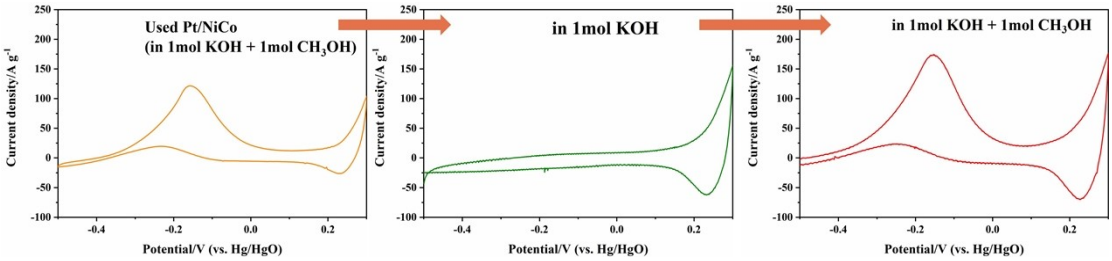

Fig.S9 CO-stripping process of Pt/NiCo.

As shown in **Fig.S9**, the MOR activity recovery rate of Pt/NiCo after CA testing (already CO-poisoned) in fresh 1M KOH is faster than that in 1M CH_3OH+1M KOH and can be restored to the high MOR activity using only one CV cycle. That is to say, the CV cycle serves as a potential window for MOR induced CO-stripping processes. The relatively high reaction kinetics of NiCo in the generation of OH_{ads} can promote the oxidation and removal process of CO_{ads} ($CO_{ads} + 2OH_{ads} \rightarrow CO_2 + H_2O$).

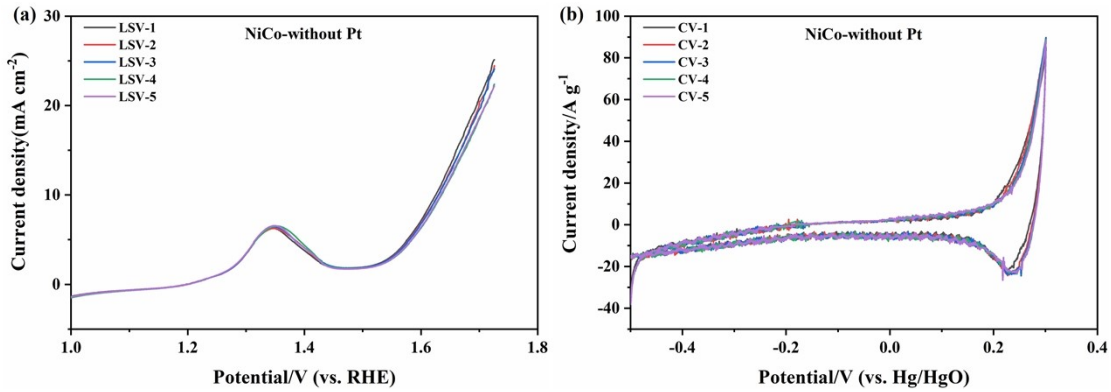

Fig.S10 (a) LSV curves and (b) CV curves of NiCo without Pt.

We redesigned the comparative experiments of NiCo alloy (without Pt) as shown in **Fig.S10**. Initially, linear scanning voltammetry was used to examine the catalyst's OER activity in a 1M KOH solution. The overpotential change trend was 474 ± 8 mV when the normalized current density was 20 mA cm^{-2}, as **Fig.S10a** illustrates. The overpotential of the NiCo alloy without Pt involvement is higher than that of the Pt/NiCo overpotential (~390 mV) depicted in **Fig.4a**. This further indicates the positive synergistic impact between Pt and NiCo. At the same time, cyclic voltammetry was used to further test the activity of MOR. It is found that the activity of NiCo alloy without Pt is very low and almost no activity, while Pt/NiCo alloy with Pt shows high activity of 495 A g^{-1}_{Pt}, as shown in **Fig.S10b** and **Fig.4b**. Compared with pure Pt (144.7 A g^{-1}_{Pt}), Pt/NiCo also exhibits the best activity. These results indicate that NiCo and Pt synergistically further improve the activity of MOR and exhibit a good ligand effect.

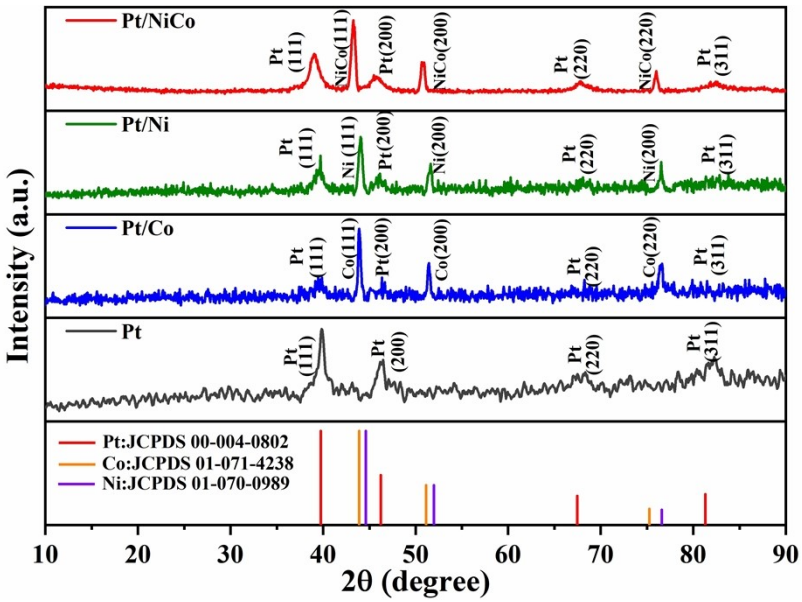

Fig.S11 XRD of Pt, Pt/Ni, Pt/Co and Pt/NiCo.

The XRD of Pt, Pt/Ni, Pt/ Co and Pt/NiCo, and the results are shown in **Fig.S11**. According to the XRD analysis, the synthesized Pt/NiCo exhibits a series of diffraction characteristic peaks, with diffraction peaks located at 40.26°, 46.86°, 68.35°, and 82.34°, respectively, attributed to the (111), (200), (220), and (311) crystal planes of Pt, and the remaining at 44.45°, 51.75°, and 76.42° attributed to the (111), (200), and (220) crystal planes of the NiCo alloy phase. Compared with the XRD patterns of pure Pt, Pt/Ni and Pt/Co samples, the positions of the peaks of Pt/NiCo patterns are all slightly skewed to the right. The reason may be caused by the effect of the alloy phase formed by NiCo and the atomic radius of Pt being larger than that of Ni and Co.

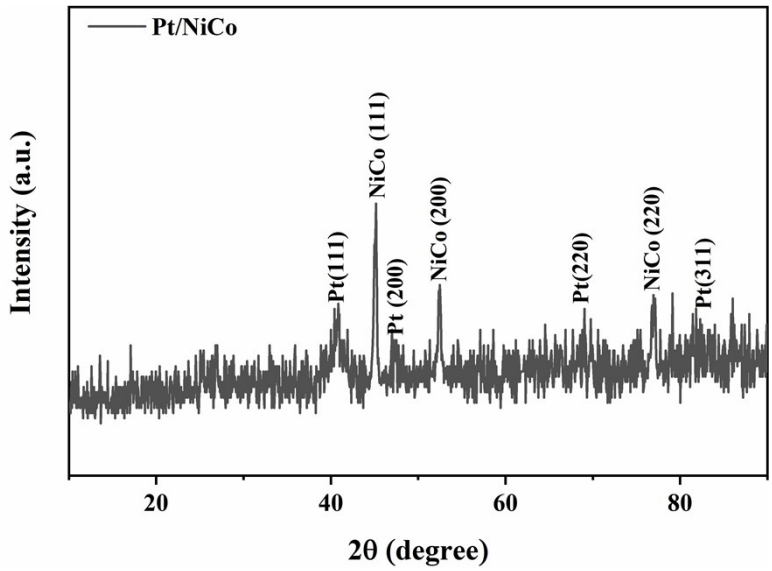

Fig.S12 XRD of Pt/NiCo after the reaction.

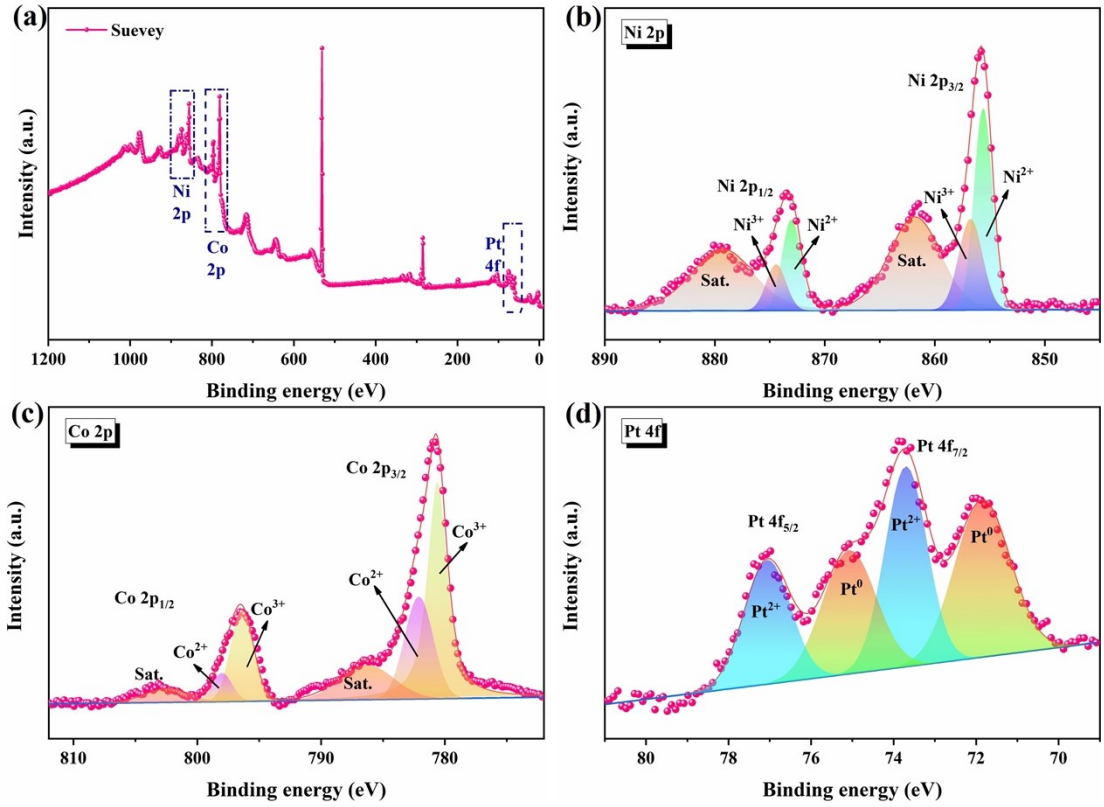

Fig.S13 XPS of Pt/NiCo after the reaction. (a) Full spectrum. (b) Ni 2p. (c) Co 2p. (d) Pt 4f.

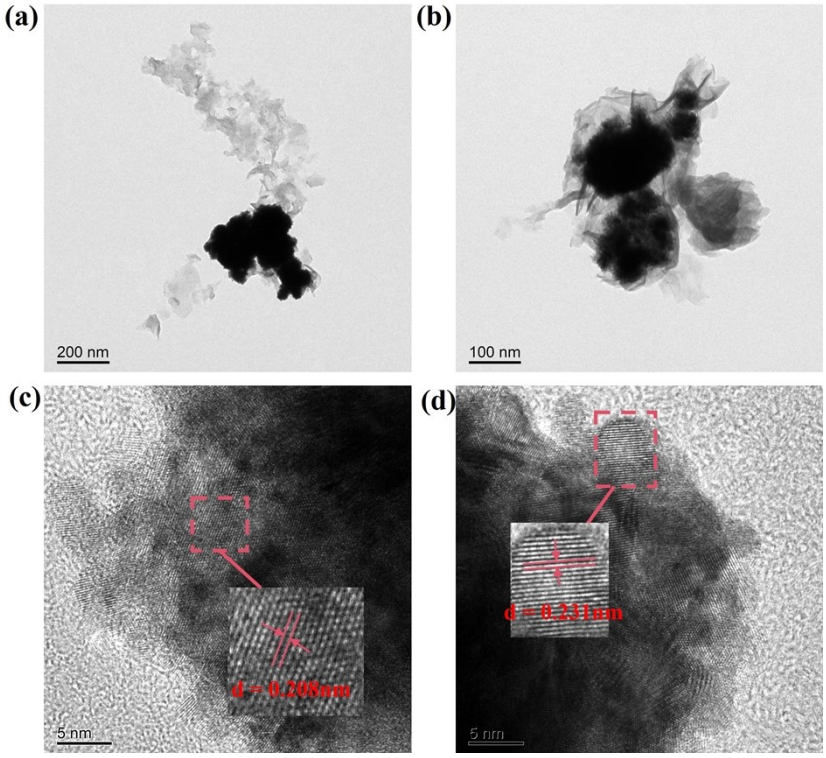

Fig.S14 TEM of Pt/NiCo after the reaction.

To further demonstrate the durability of the Pt/NiCo catalyst, XRD, XPS and TEM of Pt/NiCo after the reaction were provided. As shown in **Fig.S12** to **S14**, the XRD pattern, XPS pattern and TEM show that Pt/NiCo is stable during long-term operation. As shown in **Fig.S12** and **S14**, the XRD of Pt/NiCo after the reaction shows the same characteristic diffraction peaks of Pt and NiCo as before the reaction, The high-resolution TEM image also shows a lattice fringe of 0.208 nm corresponding to the (111) plane of the face-centered cubic (fcc) NiCo and a lattice fringe of 0.231 nm related to the (111) plane of Pt. As shown in **Fig.S13**, the XPS pattern after the reaction is similar to the initial one, but after the long-term reaction, the Pt^0 content of Pt 4f slightly decreases, and the oxidation state of Pt^{2+} becomes the dominant state of Pt 4f.

Table S1. Comparison of CV cycle stability and durability of MOR with different Pt-based catalysts.

Electrocatalyst	Durability performance	CV stability	References
This work	15000s	63.6% after 5000 cycles	/
PtPb NSs	3600s	/	[4]
PtSn NSs	1200s	48% after 500 cycles	[5]
PtCuPd@Ru	6000s	/	[6]
PdPtCu NSs	5000s	49% after 2000 cycles	[7]
hcp-PtBi/fcc-Pt	4000s	/	[8]
PtCu NTs	3600s	38.6% after 5000 cycles	[2]
Ru@Pt NWs	2000s	47.9% after 2000 cycles	[9]
Pt/NiFe-LDH/rGO	1000s	/	[10]
PtPdBi	3600s	/	[11]

Table S1 compares the CV cycle stability and durability of different Pt-based catalysts in MOR. The results show that the synthesized Pt/NiCo catalyst exhibits excellent CV cycle stability and long-term operational durability in the Pt-based catalyst. This has a more far-reaching significance for screening more stable Pt-based catalysts.

Table S2. Comparison of activity of MOR with different Pt-based catalysts.

Electrocatalyst	MOR activity	Reference
This work	495 A g^{-1}_{Pt}	/
PtRu/CNT	160 A g^{-1}_{Pt}	[12]
PtNi/FCNT	474.2 A g^{-1}_{Pt}	[13]
Pt/CeO_2 NWS	438.3 A g^{-1}_{Pt}	[14]
$Pt_3Co_1/Ti_{0.9}Ir_{0.1}O_2$	316.16 A g^{-1}_{Pt}	[15]
Pt/CrN	180 A g^{-1}_{Pt}	[16]

Pt NWs/$Ti_{0.7}W_{0.3}O_2$	355.29 A g^{-1}_{Pt}	17

References

1. T. Wang, S. Zhao, Z. Ji, L. Hao, S. Umer, J. Liu and W. Hu, *ChemSusChem*, 2023, e202300411.
2. F. Xu, S. Cai, B. Lin, L. Yang, H. Le and S. Mu, *Small*, 2022, **18**, 2107387.
3. D. Gupta, S. Chakraborty, R. G. Amorim, R. Ahuja and T. C. Nagaiah, *Journal of Materials Chemistry A*, 2021, **9**, 21291-21301.
4. L. Chen, L. Zhou, H. Lu, Y. Zhou, J. Huang, J. Wang, Y. Wang, X. Yuan and Y. Yao, *Chemical Communications*, 2020, **56**, 9138-9141.
5. J.-Y. Chen, S.-C. Lim, C.-H. Kuo and H.-Y. Tuan, *Journal of colloid and interface science*, 2019, **545**, 54-62.
6. F. Saleem, Z. Zhang, X. Cui, Y. Gong, B. Chen, Z. Lai, Q. Yun, L. Gu and H. Zhang, *Journal of the American Chemical Society*, 2019, **141**, 14496-14500.
7. H. Lv, L. Sun, D. Xu, S. L. Suib and B. Liu, *Green Chemistry*, 2019, **21**, 2367-2374.
8. Y. Qin, M. Luo, Y. Sun, C. Li, B. Huang, Y. Yang, Y. Li, L. Wang and S. Guo, *ACS Catalysis*, 2018, **8**, 5581-5590.
9. M. Li, Y. Wang, J. Cai, Y. Li, Y. Liu, Y. Dong, S. Li, X. Yuan, X. Zhang and X. Dai, *Dalton Transactions*, 2020, **49**, 13999-14008.
10. Z. Wang, F. Zhang, H. Zou, Y. Yuan, H. Wang, J. Xia and Z. Wang, *Journal of Electroanalytical Chemistry*, 2018, **818**, 198-203.
11. Z. Xiong, S. Li, H. Xu, K. Zhang, B. Yan and Y. Du, *Catalysts*, 2017, **7**, 208.
12. L. Li and Y. Xing, *The Journal of Physical Chemistry C*, 2007, **111**, 2803-2808.
13. A. B. A. A. Nassr, I. Sinev, W. Grünert and M. Bron, *Applied Catalysis B: Environmental*, 2013, **142**, 849-860.
14. Y. Chu, N. Zhang, J. Yang, H. Wang, Z. Dai, L. Wang, J. Gao and X. Tan, *Journal of Materials Science*, 2018, **53**, 2087-2101.
15. V. T. T. Phan, T. M. Pham, H. Q. Pham, T. T. Huynh, T. H. T. Nguyen and V. T. T. Ho, *International Journal of Energy Research*, 2022, **46**, 19221-19232.
16. Q. Zhou, J. Tan, W. Wang and Y. Yan, *International Journal of Hydrogen Energy*, 2023, **48**, 37258-37272.
17. H. Q. Pham, T. T. Huynh, A. T. N. Mai, T. M. Ngo, L. G. Bach and V. T. T. Ho, *Scientific Reports*, 2019, **9**, 14791.